forests

MDPI

Article

Evaluation of the Seasonal Thermal Environmental Benefits of Urban Green Space in the Core Areas of Urban Heat Island

Jiachen Liu [1], Jianting Wu [2], Yong Yang [3], Baolei Zhang [1] and Le Yin [1,*]

[1] College of Geography and Environment, Shandong Normal University, Jinan 250358, China
[2] Shandong Provincial Institute of Land Spatial Data and Remote Sensing Technology, Jinan 250014, China
[3] Shandong Provincial Territorial Spatial Ecological Restoration Center, Jinan 250014, China
* Correspondence: yinl.16b@igsnrr.ac.cn; Tel.: +86-19862148918

Abstract: The core areas of the urban heat island (CAUHI) are the most concentrated and closely associated with humans, and they are key to managing the urban heat island (UHI). It is widely acknowledged that one of the best ways to reduce the risk of UHI is the creation of urban green spaces (UGSs). However, most of the current studies are based on the grid or block scale to explore the impact of UGS on UHI. The key to mitigating the urban heat environment is to plan urban UGS rationally in the CAUHI and explore the thermal environmental benefits of UGS. This paper provides an assessment model for the thermal environmental advantages of UGS and uses ten UGS metrics as explanatory factors for seasonal land surface temperature (LST). It quantitatively evaluates the potential differences in landscape characteristics between LST and UGS under different seasons, as well as the seasonal impact on CAUHI. This study found the following: (1) The overall distribution pattern of CAUHI shows a characteristic of spreading from the central part to the surrounding area. Most of the extremely significant CAUHI is dispersed in the center and southeastern regions of the city, where there is a much greater density of impermeable surfaces and essentially no distribution of CAUHI on the natural surface represented by forest land and water bodies. (2) Except for the aggregation index (AI), correlation analysis revealed that other metrics were highly connected with LST. Among the metrics used in this study, the largest patch index (LPI) and landscape division index (DIVISION) had the highest significant correlation with LST. Patch density (PD) was strongly negatively correlated with LST, indicating that fragmented and complex UGS patches could promote vegetation cooling. (3) The green environmental benefit index (GEBI) results showed a significant degree of spatial and temporal variability in the extracted CAUHI. This study found higher GEBI values in the larger thermal patches and lower GEBI in the surrounding smaller patches. The highest mean GEBI was found in winter, at 0.6083, and the largest distribution of large high-value patches. This study revealed the geographical and temporal variability of UGS and CAUHI, and with the help of the constructed scientific evaluation model, it offered suggestions for the optimization of urban greenery.

Keywords: urban green space; thermal environment benefits; geographical detector; heat core areas; Beijing city

Citation: Liu, J.; Wu, J.; Yang, Y.; Zhang, B.; Yin, L. Evaluation of the Seasonal Thermal Environmental Benefits of Urban Green Space in the Core Areas of Urban Heat Island. *Forests* **2023**, *14*, 1500. https://doi.org/10.3390/f14071500

Received: 20 June 2023
Revised: 11 July 2023
Accepted: 14 July 2023
Published: 21 July 2023

1. Introduction

Urban expansion has brought prosperity and progress, but it has also had a negative impact on the ecological environment, particularly the thermal environment [1]. The urban heat island (UHI) [2] is a significant indicator commonly used to describe the urban thermal environment and has been the focus of academic research [3]. The UHI effect can result in adverse consequences, such as changes in species composition and distribution, increased water and energy consumption, reduced environmental quality, elevated morbidity and mortality from heat-related illnesses, and detrimental impacts on human and environmental health in urban areas [4,5]. Numerous studies have indicated that the UHI effect is

influenced by land cover type, with densely built structures exacerbating the UHI effect, while urban vegetation offers shading and transpiration, thereby mitigating the UHI effect. Moreover, increasing the extent of vegetation can alleviate the size and intensity of local heat islands [6–8].

As one of the most effective elements for controlling microclimate in urban environments, urban green space (UGS) is considered a viable option. Previous studies have demonstrated a positive correlation between impervious area and land surface temperature (LST), as well as a negative correlation between other UGS indicators [9,10]. Spatial planning and landscape composition can significantly impact surface UHI effects [11,12]. It has been observed that higher landscape fragmentation within UGS leads to lower quality in terms of species protection and cooling. Additionally, landscape configurations with larger patch sizes are more effective in reducing surface temperatures, while those with fewer connected patches have adverse effects on bioenergy exchange and biodiversity conservation [13–15]. Previous studies [16,17] that developed UGS assessment criteria solely relied on statistical analysis of landscape indicators, lacking integrated quantitative investigations within the actual urban environment. Therefore, it is crucial to determine the influence of various landscape indicators on the environmental benefits of UGS, considering the type and scale of such impacts.

In order to assess the intricate spatial organization and positive impacts of cities on the environment, it is necessary to utilize landscape indicators for analyzing the complex spatial structure and environmental benefits of UGS. However, relying solely on a single landscape indicator is inadequate for a comprehensive evaluation of the landscape and ecological quality of UGS. It requires interpretation in conjunction with related indicators [18]. Several studies have evaluated the most effective combination of indicators for specific scenarios and have suggested that the selection of indicators to quantify spatial patterns and ecological quality should be relatively simple and encompass key factors [19]. Tian et al. [20] employed nine landscape indicators that represent different UGS characteristics to construct an ecological quality index using principal component analysis and stepwise linear regression. These studies serve as valuable references for establishing evaluation indices for UGS.

Currently, there have been more studies conducted on the urban thermal environment at large scales and areas [21]. However, fewer studies have focused on the spatial and temporal characteristics of small-scale central cities, and even fewer have examined the urban thermal environment in core areas at small and medium scales. Some studies [22,23] have indicated that the core areas of UHI exert a greater impact on human activities compared to the entire urban areas. Therefore, the rational planning and management of the urban thermal environment in central urban areas play a crucial role in mitigating the heat island effect in the surrounding urban areas. With the advancement of remote sensing technology, many scholars have begun to utilize remote sensing data to investigate how UGSs alleviate the influence of UHI [24,25]. Currently, landscape models and vegetation cover are commonly employed methods for studying the heat island effect. However, these methods represent traditional approaches to obtaining remote sensing images. The emergence of the Google Earth Engine (GEE) has revolutionized the conventional way of acquiring information from remote sensing software and addressed issues related to utilizing cloud-covered images, enabling a more effective analysis [26].

Beijing is one of the most urbanized cities in China. In the context of global warming, the number of days with extreme high temperatures in the city has significantly increased in recent years. For this study, the area within the fourth ring road, which is located in Beijing's core metropolitan area and frequently experiences severe UHI effects, was selected. Additionally, the study area has a scattered distribution of urban parks, making it suitable for this research. To investigate potential differences in landscape metrics between LST and UGS across various seasons, as well as the seasonal impacts on the core areas of urban heat islands (CAUHI), ten UGS metrics were chosen. Furthermore, a composite metric called the green environmental benefit index (GEBI) was introduced to quantitatively

assess and characterize the quality of UGS in mitigating LST within the CAUHI. The primary goals of this study were as follows: (1) To identify and analyze the spatial and temporal distribution patterns of CAUHI in different seasons; (2) To determine the relative importance of explanatory variables in different seasons through correlation and regression analysis; (3) To establish a comparison matrix based on the q-values of each indicator in different seasons obtained from Geodetector, calculate the weight values of each indicator, and construct a model to identify UGS indicators with environmental benefits in different seasons, providing a UGS planning strategy. Figure 1 showed the abbreviations used in this study.

Nomenclature

CAUHI	Core areas of urban heat island
UHI	Urban heat island
LST	Land surface temperature
GEBI	Green environmental benefit index
GEE	Google Earth Engine
MSPA	Morphological spatial pattern analysis
SUHI	Surface urban heat island
PD	Patch density
LPI	Largest patch index
LSI	Landscape shape index
AREA_MN	Area-weighted mean patch size
SHAPE_AM	Area-weighted mean shape index
FRAC_AM	Area-weighted patch fractal
ENN_MN	Area-weighted Euclidean nearest neighbor distance
AI	Aggregation index
DIVISION	Landscape division index
SPLIT	Splitting index

Figure 1. Nomenclature in the study.

2. Data and Methodology

2.1. Study Area

Beijing is the capital of China (39.4°–41.6° N, 115.7°–117.4° E) and has a typical continental monsoon climate (Figure 2), with an average temperature of 13.60 °C in Beijing in 2021. With the continuous expansion of Beijing's impervious area, the city's resident population had reached 21.89 million by the end of 2021 [27]. The municipal administration of Beijing has made significant efforts in recent years to enhance the city's green spaces, resulting in a per-person green park area of 16.60 m^2 and an urban greening coverage rate of 49.00% in 2020. Given Beijing's concentric pattern of expansion, this study defines the study area as the region within Beijing's fourth ring road [28].

2.2. Datasets

In this study, we selected Landsat series data with a high spatial resolution of 30 m and good temporal continuity to conduct urban surface temperature inversion in the Google Earth Engine (GEE) for Beijing, taking into account data availability. To cater to various data

processing and analysis requirements of users, we opted for the Mono-Window Algorithm, which offers abundant datasets and robust post-combination computing capabilities. The average surface temperatures during the four seasons of spring (March–May), summer (June–August), autumn (September–November), and winter (December–February) in 2020 were utilized in this research.

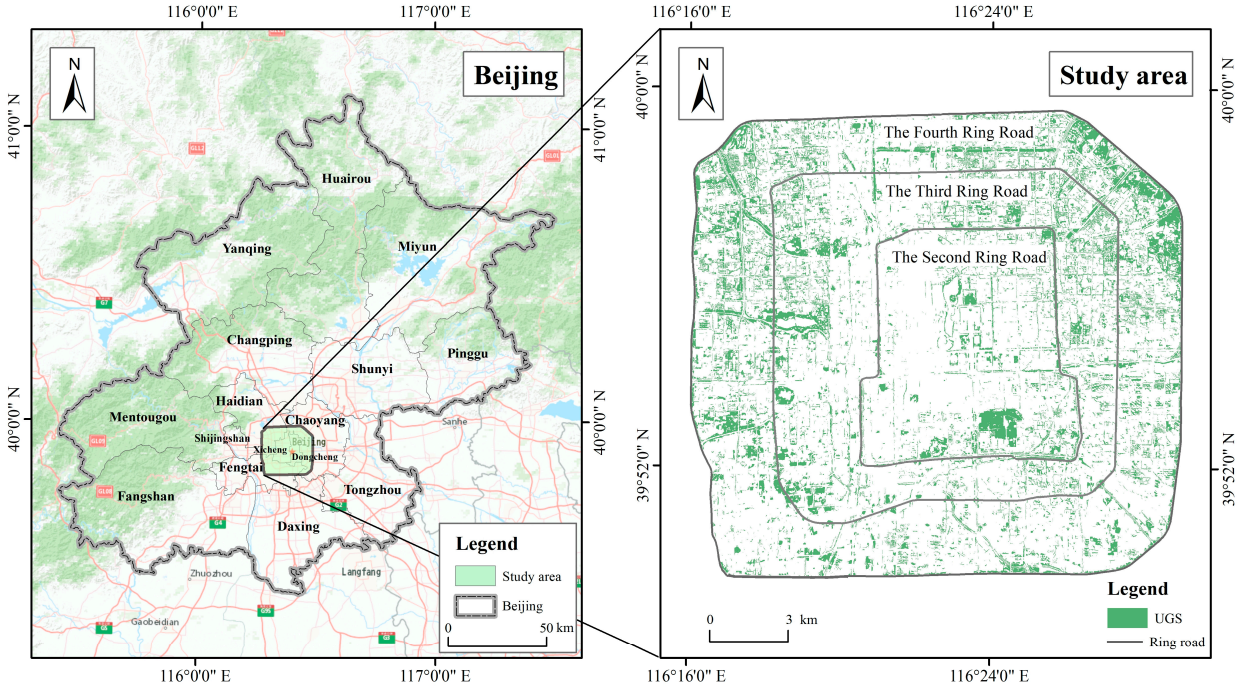

Figure 2. Location map of the study area.

The land use data utilized in this study are obtained from the World Cover dataset. This dataset, produced and published by the European Space Agency in collaboration with various scientific institutions worldwide, provides a land cover classification with a precision of 10 m. Leveraging Sentinel-1 and Sentinel-2 data, this product encompasses 11 distinct land cover categories and has undergone independent validation, achieving an overall global accuracy of approximately 75%. In our study, we categorized tree cover, shrubland, grassland, and cropland as urban green space [29].

2.3. Methodology

In this study, Landsat 8 remote sensing data were employed to conduct LST inversion in the Beijing city center. The CAUHI (composite urban heat island) was subsequently derived using the morphological spatial pattern analysis (MSPA) approach. Additionally, each CAUHI's average LST and a range of landscape metrics that utilized the CAUHI as the landscape level were computed for further statistical analysis. To estimate the weights of each UGS (urban green space) measure, the analytic hierarchy process method was employed for model construction and analysis, based on Geodetector's q-value. Figure 3 illustrates the flowchart of this research.

2.3.1. LST Retrieval

The retrieval of LST (unit: °C) was accomplished by utilizing the surface thermal radiation data collected by the TIRS 10 on Landsat-8, which is categorized into spectral bands. This approach employed a single-window algorithm and was based on previous studies by Tu et al., Wang et al., and Yu et al. [25,30]. The calculations involved four key parameters, namely atmospheric transmittance (τ), brightness temperature (T10), mean

atmospheric temperature (T_a), and land surface emissivity (ε), which were incorporated using Formulas (1)–(4):

$$T_S = \frac{a(1-C-D)+[b(1-C-D)+C+D]T_b - DT_a}{C} \quad (1)$$

$$C = \varepsilon \times \tau \quad (2)$$

$$D = (1-\tau)[1+(1-\varepsilon)\tau] \quad (3)$$

$$T_a = 16.0110 + 0.92621T_0 \quad (4)$$

where a and b are coefficients obtained from the relationship between thermal radiation intensity and brightness temperature, a = −67.35535, b = 0.45861. The National Aeronautics and Space Administration (NASA, http://atmcorr.gsfc.nasa.gov) provided the atmospheric transmittance (τ).

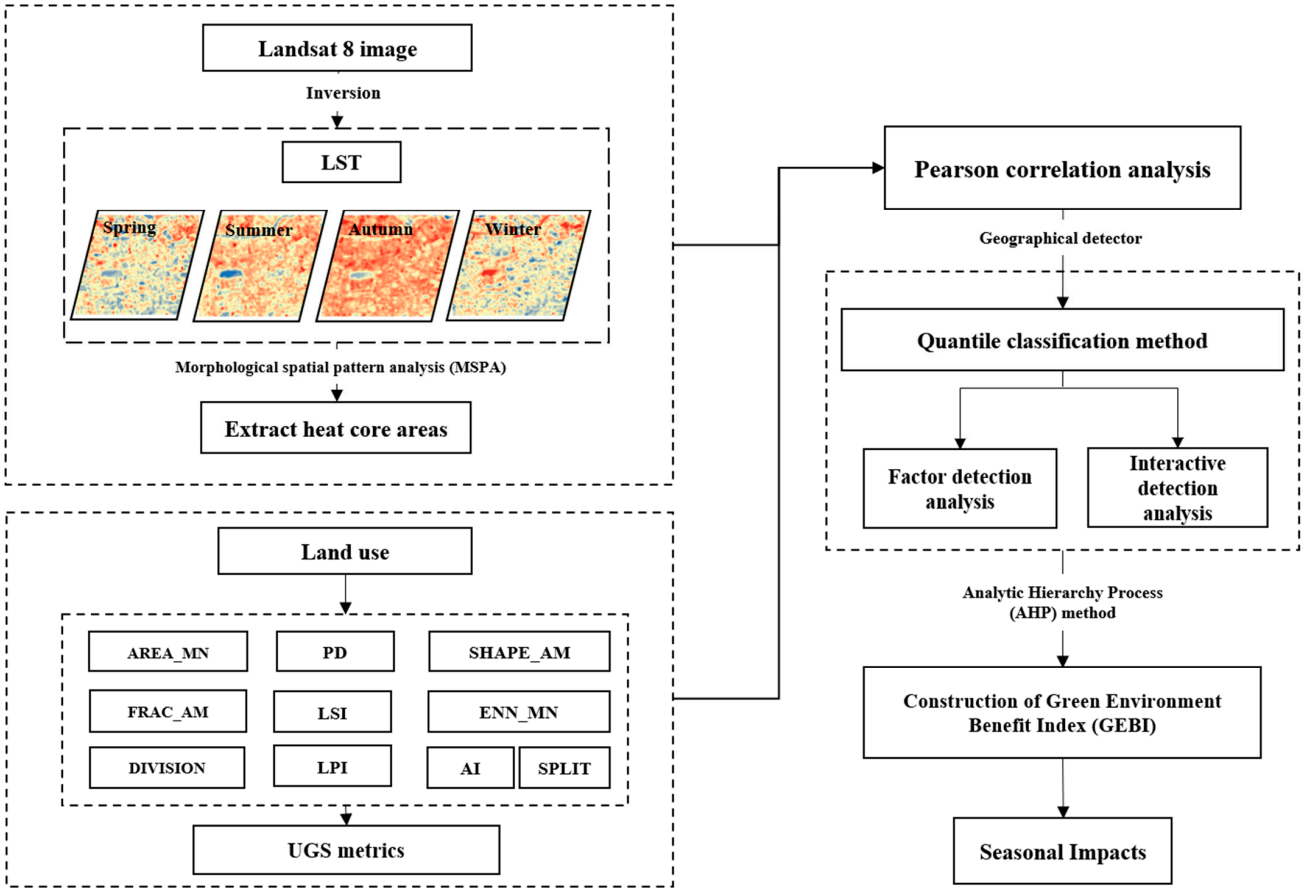

Figure 3. Research framework.

2.3.2. The Identification of CAUHI

In this study, due to the high degree of economic development and substantial impervious in the study area, it is more acceptable to use land cover data to distinguish between rural and urban areas, and LST_{rural} was derived as the LST mean of suburban image elements in the land cover data (rural areas are defined here as locations other than impervious, lake bodies, and mountainous areas) [31]. Surface urban heat island (SUHI) reduces the effects of local meteorological conditions and other sources of inaccuracy since it measures temperature differentials rather than absolute temperatures [32].

UHI patches can be quantified using the urban–rural dichotomy, a widely used approach for identifying *UHI*, and *SUHI*, which is determined as the difference in *LST* between urban (LST_{urban}) and rural (LST_{rural}) pixels. The calculation formula is as follows:

$$SUHI = LST_{urban} - LST_{rural} \quad (5)$$

For the purpose of creating a binary map, the demarcated *UHI* patches were used as backdrop values. The MSPA method was used to calculate the results with the aid of Guidos Toolbox software, and the core areas were extracted as CAUHI. Based on mathematical morphology, Peter Vogt [33] created the MSPA method to recognize and categorize the morphological spatial patterns of matching images [34,35]. UGS cannot be indefinitely increased due to policy and funding constraints, as implementing the most effective UGS policy in the most central locations can go a long way to alleviating the *UHI* phenomenon. This paper will use the core area extracted from the MSPA as the CAUHI and use this as the unit of study to explore the cooling benefits of UGS (Figure 4).

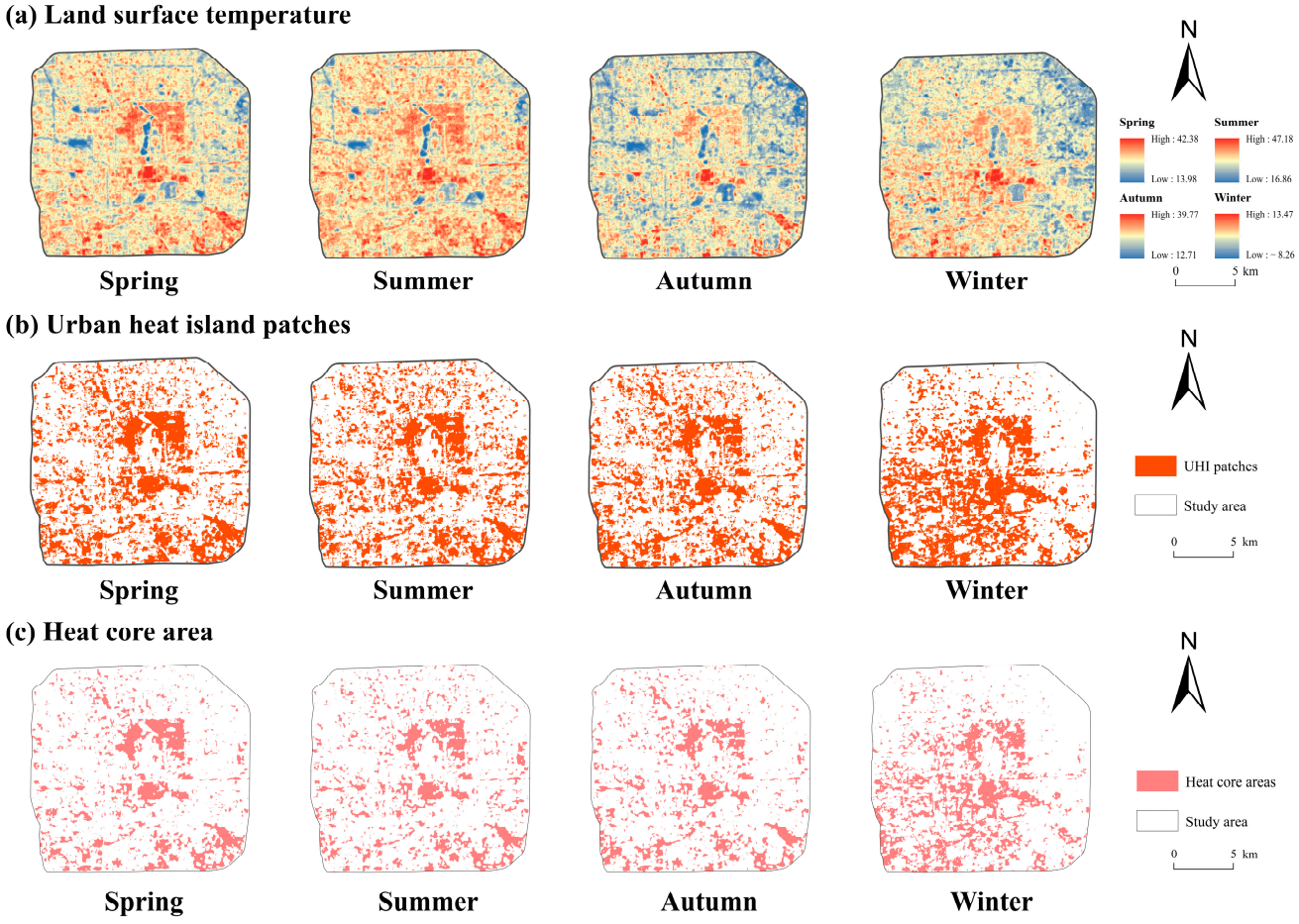

Figure 4. Extraction process in the CAUHI of the study area.

2.3.3. UGS Metrics

We conducted research analysis in the retrieved CAUHI based on the UGS distribution and research requirements. The mean LST of each CAUHI and a number of landscape metrics that use the CAUHI as the landscape level are then extracted for further statistical analysis. With reference to thorough research on the usefulness of landscape metrics and their use in urban thermal environment studies, we chose 10 metrics (Table 1) to measure the UGS landscape grid [32,34].

Table 1. Introduction of UGS metrics used in this study.

Metrics	Abbreviation	Description	Formula	Unit
Patch density	*PD*	*PD* represents the density of patches of UGS	$PD = \frac{n_i}{A}(10,000)(100)$	Number per 100 hectares
Largest patch index	*LPI*	The largest patch of UGS patch	$LPI = \frac{\max\left(a_{ij}\right)}{A}(100)$	Percent
Landscape shape index	*LSI*	Landscape shape index of UGS patch	$LSI = \frac{E}{minE}$	——
Area-weighted mean patch size	*AREA_MN*	Mean patch size of the corresponding patch type	——	Hectare
Area-weighted mean shape index	*SHAPE_AM*	*SHAPE_AM* represents the area-weighted average shape index of UGS	——	——
Area-weighted patch fractal	*FRAC_AM*	FRAC_AM reflects shape complexity	——	——
Area-weighted Euclidean nearest neighbor distance	*ENN_MN*	It is the ENN-MN weighted by the relative area of patches	$ENN = \frac{\sum_{i=1}^{m}\sum_{j=1}^{n} h_{ij}}{N}$	Meter
Aggregation index	*AI*	AI represents the degree of aggregation between landscape patches	$AI = \left\lvert \frac{g_{ii}}{max \to g_{ii}} \right\rvert (100)$	Percent
Landscape division index	*DIVISION*	Landscape division index of UGS patch	$DIVISION = 1 - \sum_{i=1}^{m}\sum_{j=1}^{n} (\frac{a_{ij}}{A})^2$	——
Splitting index	*SPLIT*	Splitting index of UGS patch	$SPLIT = \frac{A^2}{\sum_{i=1}^{m}\sum_{j=1}^{n} a_{ij}^2}$	——

i = type of patches; j = 1, . . ., n patches; A = the area of patches; h_{ij} = distance based on edge-to-edge measurements between two patches that are closest to one another; N = number of patches; n_i = number of patches in the landscape of patch type; a_{ij} = the area of patch ij; E = total edge length with respect to the landscape after the number of cell surfaces; $minE$ = Minimum overall edge length considering the number of cell surfaces; g_{ii} represents joins between pixels concerning patch type 'i'; $\max \to g_{ii}$ represents the maximum joins between pixels concerning patch type 'i'.

2.3.4. The Green Environmental Benefit Index Model

This study modeled the green environmental benefit index of UGS based on the results of correlation analyses and regression analyses, quantifying the relationship between UGS and LST using equations. Therefore, this study used the Pearson correlation test to select UGS metrics that were statistically significant for LST (Table 1), and the R value generated by this test helped to identify UGS metrics that had the potential to influence LST. The correlation test also provided a mechanism for whether these UGS metrics were statistically independent of each other. In this study, the individual UGS metrics were factor-tested with Geodetector, and a comparison matrix was built utilizing Saaty's 1–9 scale approach and the findings of the factor testing. Finally, the model equations were constructed using the analytic hierarchy process (AHP) to determine the weights of each indicator based on the constructed comparison matrix:

$$GEBI = a_0 + a_1X_1 + a_2X_2 + a_3X_3 + \ldots + a_nX_n \quad (6)$$

where *GEBI* is the green environmental benefit index; a_1, a_2, . . ., a_n are the weights of each UGS indicator; and X_1, X_2, . . ., X_n are the UGS normalized metrics. To eliminate differences in scaling and order of magnitude between the various UGS metrics, the index data are normalized:

$$X_i = \frac{x_i - \overline{x}_i}{\sigma_i} \quad (7)$$

X_i is the UGS normalized indicator; i represents the type of UGS indicator; x_i is the value of the UGS indicator; $\overline{x}_i$ is the mean value; and σ_i represents the standard deviation.

3. Results

3.1. Seasonal Distribution of the CAUHI in Study Area

In this study, the LST of the inversion was tested by fitting the data from 12 national meteorological stations to the LST of the inverse remote sensing images, resulting in a correlation coefficient of 0.85 (Figure 5).

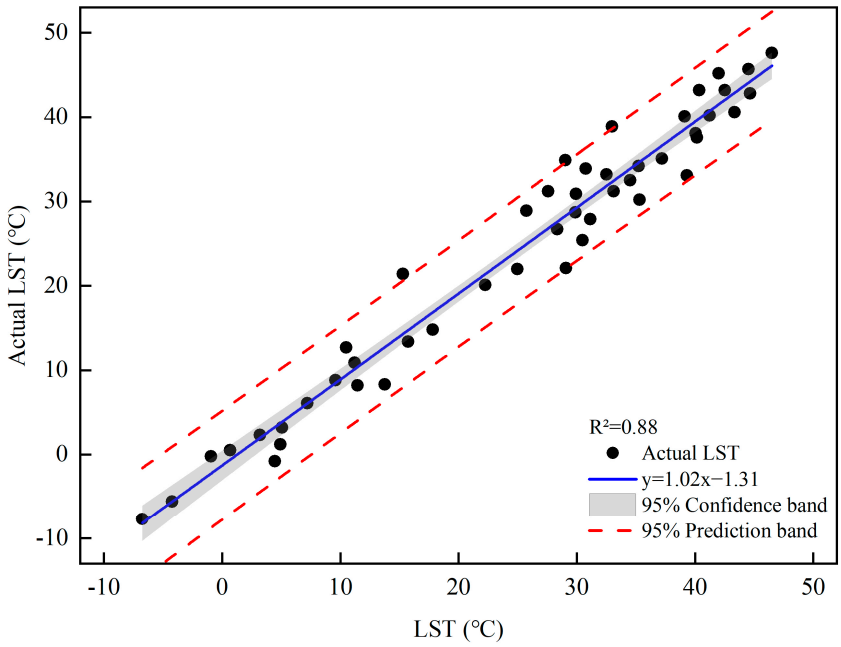

Figure 5. Correlation analysis between the remote sensing of LST and actual LST.

The findings of the CAUHI extraction were displayed in Figure 3 and represented, respectively, 16.14%, 16.20%, 16.27%, and 19.68% of the overall study area. In terms of spatial distribution, the larger, more interconnected CAUHI were primarily found in the study area's center, which fell under the purview of the east and west urban areas. The majority of the extremely significant CAUHI were distributed in the core and southeastern parts of the city, where there was a significantly higher density of impervious, and there was almost no distribution of CAUHI on the natural surface represented by forest land and water bodies. The CAUHI were less distributed due to low land development intensity and extensive forest land distribution in the north and southwest. In addition, the overall distribution pattern of the CAUHI showed a characteristic of spreading from the central part to the surrounding area. In terms of CAUHI, the identification results were similar in spring, summer, and autumn, with a more uniform size of CAUHI and a more even distribution of sporadic small CAUHI, but the average size of CAUHI was the largest and most scattered in winter. From spring to winter, CAUHI showed a trend of shifting to the southwest of the study area. The study area's winter heat risk will significantly increase due to the establishment of many big CAUHI in the middle of the study area with concealed connection patterns.

3.2. Pearson Correlation Analysis between UGS Metrics and Seasonal LST

With the exception of AI, correlation analysis revealed that all measures were highly connected with LST. From a seasonal perspective, AREA_MN in summer, PD in autumn, and FRAC_AM in winter also showed non-significant correlations with LST. Among the metrics used in this study, LPI and DIVISION were the two metrics with the highest significant correlation with LST. Of these, LPI was negatively correlated with LST, with 4 seasonal correlation coefficients of −0.561, −0.525, −0.577, and −0.463, respectively. DIVISION was positively correlated with LST, with correlation coefficients of 0.561, 0.542, 0.569, and 0.465 for the 4 seasons. In addition, LSI, SHAPE_AM, and SPLIT also showed relatively high correlations with LST, all showing positive correlations. The data above showed that when the aggregation of UGS patches grew, the cooling effect enhanced. This study discovered that the best cooling impact was produced by massive planting aggregates dispersed throughout intricate, uniformly structured UGS. The substantial negative correlation between PD and LST suggests that complex and fragmented UGS patches may facilitate vegetation cooling.

We produced scatter plots of the mean LST and UGS measurements in the CAUHI cell in order to better comprehend the data. Figure 6 demonstrated the non-linear connection between PD, SPLIT, FARC_AM, and AI and LST. Additionally, because diverse UGS measures interact in the urban setting, the impact of UGS upon the urban thermal environment is more complicated, necessitating additional investigation using Geodetector.

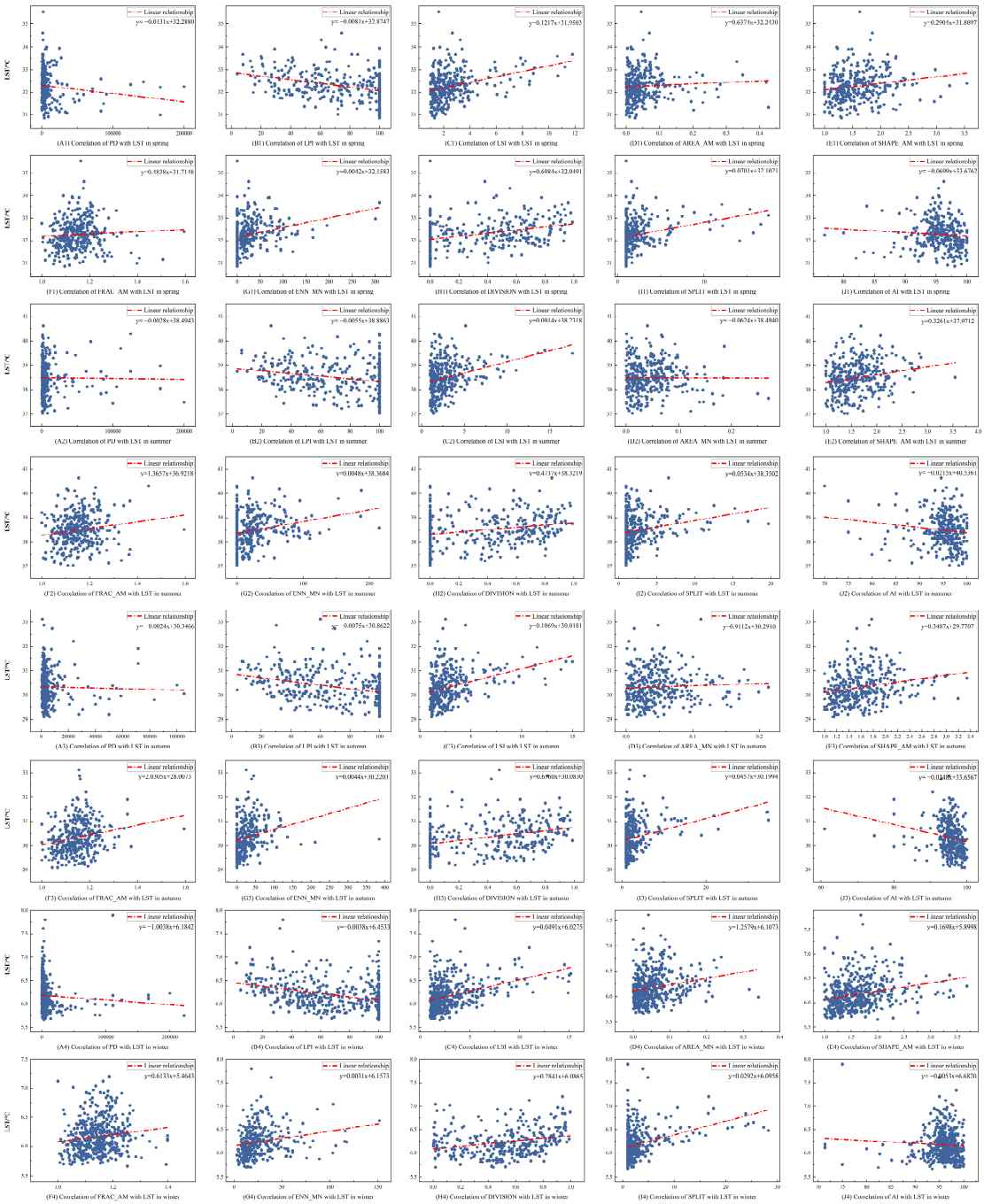

Figure 6. The scatterplot of different UGS metrics versus LST for different seasons. Where A-J represent the 10 UGS metrics and 1–4 represent the seasons.

3.3. Analysis of UGS Metrics Influencing Seasonal LST based on Geodetector

The driving effects of the 10 UGS metrics were quantified using Geodetector for all 4 seasons as drivers of LST, all with *p*-values < 0.001. In spring, their explanations for the spatially stratified variety of LST were in the following order: AI > SHAPE_AM > FRAC_AM > PD > LSI > AREA_MN > LPI > SPLIT > ENN_MN > DIVISION (Table 2). In summer, its

explanation rate for LST spatial stratification heterogeneity was in the following order: AI > PD > FRAC_AM > SHAPE_AM > AREA_MN > LSI > SPLIT > LPI > DIVISION> ENN_MN. In autumn, its explanation rate for LST spatial stratification heterogeneity was in the following order: AI > PD > LSI > SHAPE_AM > FRAC_AM > AREA_MN > LPI > SPLIT > ENN_MN > DIVISION. In winter, its explanation rate for LST spatial heterogeneity was AI > PD > SHAPE_AM > FRAC_AM > LSI > AREA_MN > LPI > SPLIT > DIVISION> ENN_MN.

Table 2. Results of factor detector between UGS metrics and LST.

Season	PD	LPI	LSI	AREA_MN	SHAPE_AM	FRAC_AM	ENN_MN	DIVISION	SPLIT	AI
Spring	0.908	0.595	0.899	0.816	0.943	0.937	0.587	0.585	0.595	0.978
Summer	0.928	0.636	0.824	0.835	0.902	0.913	0.632	0.632	0.639	0.971
Autumn	0.951	0.779	0.939	0.859	0.939	0.938	0.770	0.768	0.779	0.967
Winter	0.894	0.688	0.842	0.819	0.859	0.853	0.666	0.679	0.686	0.924

The UGS metric interaction detector's findings (Figure 7) show that each pair of UGS metrics' interaction enhanced the seasonal impact of each individual element on LST. In the autumn, q($PD \cap LSI$), q($PD \cap SHAPE\_AM$), q($PD \cap FRAC\_AM$), q($PD \cap AI$), q($LSI \cap AREA\_MN$), q($AREA\_MN \cap SHAPE\_AM$), q($AREA\_MN \cap FRAC\_AM$), q($AREA\_MN \cap AI$), q($SHAPE\_AM \cap FRAC\_AM$), and q($FRAC\_AM \cap AI$) had the highest values, all at 0.9915.

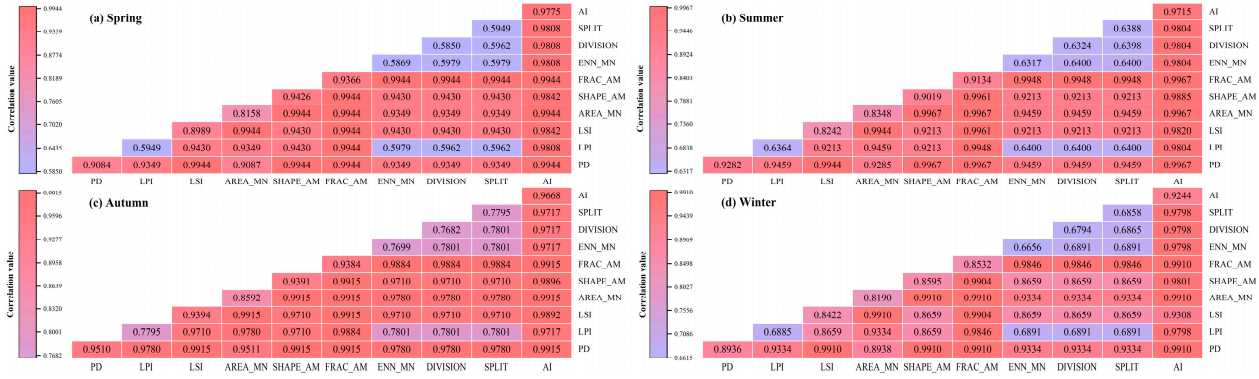

Figure 7. (**a**). represents the interaction of the spring UGS metrics with LST in detector; (**b**). represents the interaction of the summer UGS metrics with LST in detector; (**c**). represents the interaction of the autumn UGS metrics with LST in detector; (**d**). represents the interaction of the winter UGS metrics with LST in detector.

Although AI was not significantly correlated in the correlation analysis, AI, SHAPE_AM, and PD had higher explanatory rates for factor detection, while the interaction between the PD, AI, and SHAPE_AM had strong effects, indicating that the combined consideration of AI, SHAPE_AM, and PD could yield higher UGS to mitigate the UHI effect. The findings of the interaction experiments demonstrate that, when the total area of UGS is constrained, increasing the variety and connection of all species of plants and lowering the irregularity of patch forms are preferable strategies to maximize greenery.

3.4. Thermal Environmental Benefits Evaluation of UGS

The concept of Saaty's 1–9 scale technique and the findings of factor identification were used in this study to establish the general methodology for building the comparison matrix: if the variable's q-value C_i differs from the q-value of C_j by 0–0.1, the value of (C_i, C_j) is assigned as 2 and the value of (C_j, C_i) is 1/2. Two-by-two comparison matrices are obtained according to the above principles.

In this study, weights were calculated using the AHP method with the help of MATLAB software, and the final formulas for calculating the *GEBI* for each season are in Table 3.

Table 3. Calculation formulas of *GEBI* in each season.

Season	Formula
Spring	$GEBI$ =0.1315 × PD + 0.0329 × LPI + 0.1147 × LSI + 0.0818 × AREA_MN + 0.1821 × SHAPE_AM + 0.1588 × FRAC_AM+0.0270 × ENN_MN + 0.0236 × DIVISION + 0.0387 × SPLIT + 0.2089 × AI
Summer	$GEBI$ =0.1751 × PD + 0.0378 × LPI + 0.0782 × LSI + 0.1074 × AREA_MN + 0.1455 × SHAPE_AM + 0.1266 × FRAC_AM+0.0279 × ENN_MN + 0.0321 × DIVISION + 0.0434 × SPLIT + 0.2259 × AI
Autumn	$GEBI$ =0.1649 × PD + 0.0527 × LPI + 0.1433 × LSI + 0.0750 × AREA_MN + 0.1246 × SHAPE_AM + 0.1083 × FRAC_AM+0.0435 × ENN_MN + 0.0378 × DIVISION + 0.0527 × SPLIT + 0.1972 × AI
Winter	$GEBI$ =0.1752 × PD + 0.0501 × LPI + 0.1200 × LSI + 0.0877 × AREA_MN + 0.1381 × SHAPE_AM + 0.1044 × FRAC_AM+0.0329 × ENN_MN + 0.0378 × DIVISION + 0.0435 × SPLIT + 0.2103 × AI

This study analyzed the *GEBI* results on extracted CAUHI and found a high degree of spatial and temporal heterogeneity (Figure 8). This study found higher *GEBI* values in the larger thermonuclear patches and lower *GEBI* in the surrounding smaller patches. The maximum value of *GEBI* occurred in the spring of 2020 with 0.7195 and the minimum value occurred in the winter with only 0.6763, but we found the highest mean *GEBI* also in the winter with 0.6083 and the largest distribution of large high-value patches. This indicates that the average cooling effect of green space is best in winter. Comparing the land use map of the study area, we can find that although the largest *GEBI* occurs in the largest heat core patches, these also have the largest distribution of green space area, which indicates that expanding the area of green space and increasing the connectivity of green space is the best way to cool the *UHI*.

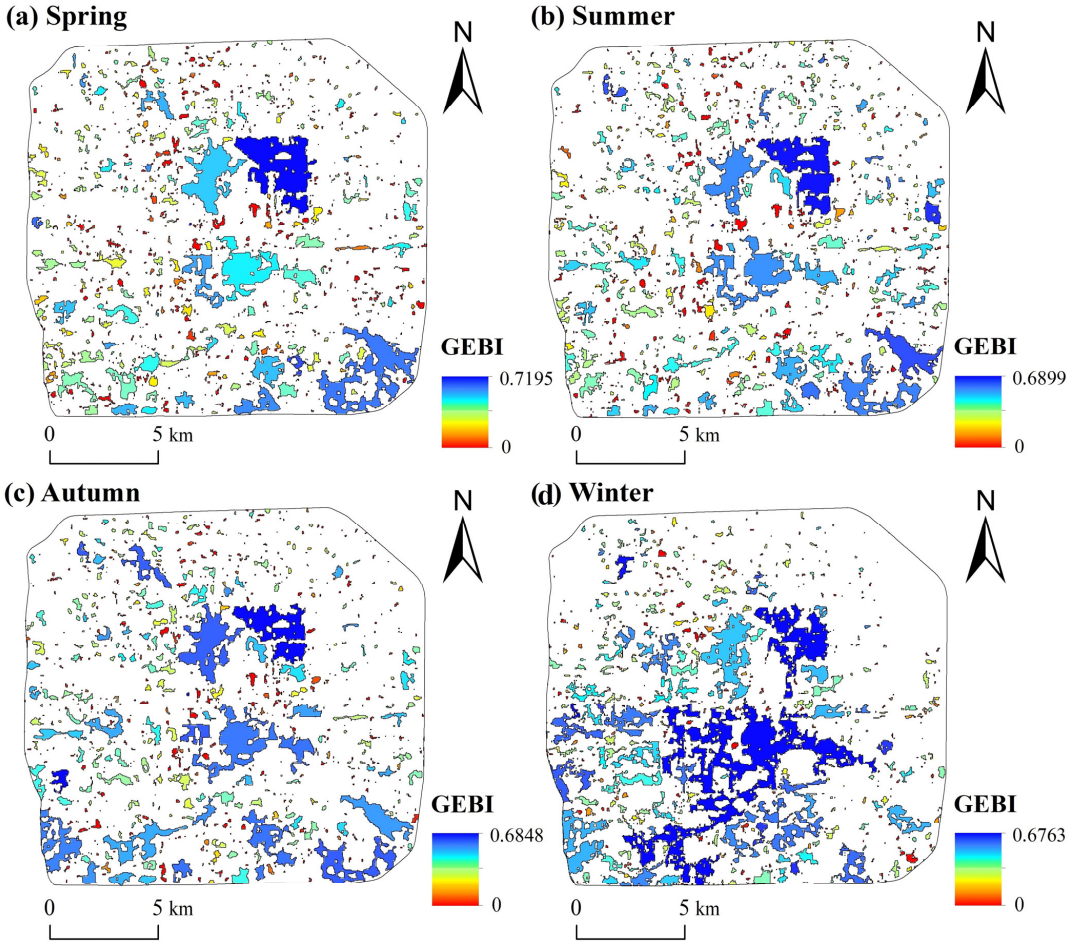

Figure 8. Spatial and temporal distribution of *GEBI*.

4. Discussion

4.1. Influence of the UGS Metrics on Seasonal LST

This study investigated the impact of UGS on LST and the seasonal variation in the CAUHI. The results demonstrated that the landscape pattern of UGS within the study area significantly influenced LST, with varying effects depending on the distribution of UGS landscape patterns [28,36]. The selected green areas' landscape pattern indices in the main urban regions of Beijing exhibited significant correlations with LST (except for AI). Furthermore, the UGS's LSI exhibited a significant positive correlation with LST, suggesting that a more complex shape of landscape patches led to a weaker reduction in LST, consistent with the findings of Yao et al. [37] that simpler UGS patches resulted in lower LST. This study also found a positive correlation between SPLIT and LST, aligning with the findings of Li et al. [38]. While the study by Bao et al. [39] focused on larger UGS areas and neglected smaller UGS patches, parks were considered equally important in urban areas. On the other hand, some other studies [6] employed homogeneous grids. According to our study, evenly spaced and well-distributed UGSs were more effective in mitigating the UHI effect.

Generally, this study confirmed the significant role of UGS in reducing LST in CAUHI. It has aligned with previous studies [37] that have highlighted the importance of landscape planning and spatial configuration features of UGS in minimizing the extent of the urban thermal environment [40]. Moreover, it has been observed that UGS has been able to provide diverse climate regulation functions based on different landscape characteristics, including types and configurations [41,42]. For instance, contrary to the findings of Yao et al. [37] suggesting a positive relationship between PD of UGS and average LST, this study has taken into account the similarity of UGS patches and has revealed a strong negative correlation between PD of UGS and LST. In the broader scope of the entire UHI region, landscape metrics associated with UGS made a more substantial contribution to LST, with some studies emphasizing the significance of landscape composition over landscape design [43,44].

4.2. Evaluation of the Thermal Environmental Benefits of the Model

The UGS landscape pattern has a significant impact on the urban thermal environment, according to the majority of scholars who have studied its drivers. However, few studies have focused on CAUHI [38]. Previous studies [22,23] have revealed a hotter core in the UHI. CAUHI affect people the most and is a crucial area for reducing the UHI. Satellite observation can provide a feasible method to more accurately examine the UHI structure with many hotspots having higher LST within the boundaries of a large-scale UHI [45]. This study suggests that Geodetector can be a useful tool for examining the interactions and impacts of UGS landscape elements on the urban thermal environment. Based on the results of the UGS survey on the driving impact of LST, the evaluation metrics and weights for the UGS evaluation model were developed using the explanation rate of each element provided by Geodetector as a criterion [46]. The *GEBI* proposed in this research was developed based on a thorough investigation of the actual reaction from the urban environment to various UGS landscape styles. Landscape metrics can serve as a convincing and understandable basis for evaluating UGS if it has been clearly determined which landscape elements are helpful in enhancing the cooling effect of UGS. However, the results of the Geodetector analysis, which are connected to the unique features of the research region, can influence the selection and weighting of landscape metrics.

Quantification of the UGS revealed that larger values of the *GEBI* were distributed across extensive patches of CAUHI, with the Dongcheng and Xicheng areas being particularly prominent. The widespread distribution of UGS on these large patches, along with the high number of UGS patches, indicated that implementing extensive greening in the CAUHI was the right decision to achieve a better cooling effect. This study demonstrated the valuable use of Geodetector as a tool to investigate the various effects and interactions of UGS metrics on the urban thermal environment [9]. The interpretation rate of each component provided by Geodetector served as a metric for selecting evaluation metrics

and weights based on the identification of LST-driven impacts using UGS metrics. Previous evaluation models relied solely on statistical correlations between metrics, and evaluation metrics were developed through principal component analysis or factor analysis on different landscape data [46]. In comparison, this study developed a more objective and useful assessment model by incorporating the environmental advantages of multiple UGS metrics in the CAUHI. This study presented an effective UGS evaluation model based on the CAUHI of the urban thermal environment [24]. During the actual implementation of this study, certain details could be effectively adjusted: (1) Different categorization approaches, such as more precise divisions based on areas with trees and grasses, can be utilized to classify UGS. It has been previously established that there are variations in the cooling effects of trees, shrubs, and grasses, with a decreasing trend in the cooling effect from trees to shrubs to grasses [47]. (2) Based on the results of the Geodetector study, the construction guidelines for the comparison matrix in the AHP method can be modified.

4.3. Limitations

First of all, although this study utilized LST data captured during nighttime, it is important to consider the daily maximum temperature, which occurs between 14:00 and 16:00 in the afternoon. Therefore, additional consideration is needed regarding the warming or cooling impact of the urban landscape during this time [48]. Three-dimensional factors such as topography, building height, and vegetation coverage also have a significant influence on thermal diffusion. Hence, these factors should be taken into account when constructing the friction map. It is important to consider three-dimensional characteristics, including terrain, building heights, and vegetation cover, as they greatly affect heat diffusion [49,50]. Additionally, this model has a limited selection of UGS metrics and may overlook some metrics that are essential to the urban thermal environment. However, the urban CAUHI was chosen for this study, posing challenges in selecting appropriate testing scales.

5. Conclusions

Regression analysis was performed in this work to examine the connection between UGS metrics and LST. The evaluation model developed compared the impact of UGS metrics across the central city and calculated their thermal environmental benefits for the CAUHI. The overall distribution pattern of the CAUHI showed a characteristic of spreading from the central part to the surrounding area, and the majority of the city's highly significant CAUHI were located in the southeast and center. With the exception of AI, all indicators had a strong correlation to LST. The cooling effect was improved as the aggregation of UGS patches increased. According to the considerable negative correlation between PD and LST, complex and fragmented UGS patches may help to cool the plant. This study found higher *GEBI* values in the larger thermonuclear patches and lower *GEBI* in the surrounding smaller patches. We analyzed the extracted CAUHI results using *GEBI* and found a high degree of spatial and seasonal heterogeneity. This study can aid in the development of a rigorous, scientific assessment methodology and serve as a guide for the design and optimization of urban greening by providing additional information about the UGS landscape pattern.

Author Contributions: Formal analysis, J.L., J.W., and B.Z.; methodology, J.L. and L.Y.; resources, Y.Y.; software, J.L. All authors will be informed about each step of manuscript processing including submission, revision, revision reminder, etc. via emails from our system or assigned Assistant Editor. All listed authors meet the ICMJE criteria and all who meet the four criteria are identified as authors. We attest that all authors contributed significantly to the creation of this manuscript, each having fulfilled the criteria as established by the ICMJE. All authors have read and agreed to the published version of the manuscript. We confirm that the order of authors listed in the manuscript has been approved by all named authors.

Funding: This research was funded by the National Social Science Foundation of China (No. 18BJY086), the National Natural Science Foundation of China (42201308), and the Natural Science Foundation of Shandong Province, China (ZR2021QD127).

Data Availability Statement: No new data were created. The availability of data and materials is based on personal requests.

Conflicts of Interest: The authors declare no conflict of interest.

References

1. Manley, G. On the frequency of snowfall in metropolitan England. *Q. J. R. Meteorol. Soc.* **1958**, *84*, 70–72. [CrossRef]
2. Oke, T.R. The energetic basis of the urban heat island. *Q. J. R. Meteorol. Soc.* **1982**, *108*, 1–24. [CrossRef]
3. Schwarz, N.; Schlink, U.; Franck, U.; Großmann, K. Relationship of land surface and air temperatures and its implications for quantifying urban heat island indicators—An application for the city of Leipzig (Germany). *Ecol. Indicators* **2012**, *18*, 693–704. [CrossRef]
4. Arnfield, A.J. Two decades of urban climate research: A review of turbulence, exchanges of energy and water, and the urban heat island. *Int. J. Climatol.* **2003**, *23*, 1–26. [CrossRef]
5. Grimm, N.B.; Faeth, S.H.; Golubiewski, N.E.; Redman, C.L.; Wu, J.; Bai, X.; Briggs, J.M. Global Change and the Ecology of Cities. *Science* **2008**, *319*, 756–760. [CrossRef] [PubMed]
6. Tang, Z.H.; Li, Y.; Gu, Y.; Jiang, W.; Xue, Y.; Hu, Q.; Li, R. Assessing Nebraska play a wetland inundation status during 1985-2015 using Landsat data and Google Earth Engine. *Environ. Monit. Assess.* **2016**, *188*, 654. [CrossRef]
7. Liu, J.; Zhang, S.; Yin, L.; Li, B.; Zhang, B. Exploring the relationship between seasonal variations of land surface temperature and urban morphological factors in complex urban areas. *Env. Sci. Pollut. Res. Int.* **2023**, *30*, 59861–59876. [CrossRef] [PubMed]
8. Liu, Y.; Wang, Z.; Liu, X.; Zhang, B. Complexity of the relationship between 2D/3D urban morphology and the land surface temperature: A multiscale perspective. *Env. Sci. Pollut. Res. Int.* **2021**, *28*, 66804–66818. [CrossRef]
9. Zhou, L.; Hu, F.; Wang, B.; Wei, C.; Sun, D.; Wang, S. Relationship between urban landscape structure and land surface temperature: Spatial hierarchy and interaction effects. *Sustain. Cities Soc.* **2022**, *80*, 103795. [CrossRef]
10. Ge, X.; Mauree, D.; Castello, R.; Scartezzini, J.-L. Spatio-Temporal Relationship between Land Cover and Land Surface Temperature in Urban Areas: A Case Study in Geneva and Paris. *ISPRS Int. J. Geo-Inf.* **2020**, *9*, 593. [CrossRef]
11. Chen, S.; Yu, Z.; Liu, M.; Da, L.; Faiz Ul Hassan, M. Trends of the contributions of biophysical (climate) and socioeconomic elements to regional heat islands. *Sci. Rep.* **2021**, *11*, 12696. [CrossRef]
12. Qiao, Z.; Wu, C.; Zhao, D.; Xu, X.; Yang, J.; Feng, L.; Sun, Z.; Liu, L. Determining the Boundary and Probability of Surface Urban Heat Island Footprint Based on a Logistic Model. *Remote Sens.* **2019**, *11*, 1368. [CrossRef]
13. Cui, L.; Wang, J.; Sun, L.; Lv, C. Construction and optimization of green space ecological networks in urban fringe areas: A case study with the urban fringe area of Tongzhou district in Beijing. *J. Clean. Prod.* **2020**, *276*, 118360. [CrossRef]
14. Han, X.; Yu, J.; Shi, L.n.; Zhao, X.; Wang, J. Spatiotemporal evolution of ecosystem service values in an area dominated by vegetation restoration: Quantification and mechanisms. *Ecol. Indic.* **2021**, *131*, 108191. [CrossRef]
15. An, H.; Cai, H.; Xu, X.; Qiao, Z.; Han, D. Impacts of Urban Green Space on Land Surface Temperature from Urban Block Perspectives. *Remote Sens.* **2022**, *14*, 4580. [CrossRef]
16. Tian, Y.; Jim, C.Y.; Wang, H. Assessing the landscape and ecological quality of urban green spaces in a compact city. *Landsc. Urban Plan.* **2014**, *121*, 97–108. [CrossRef]
17. Han, D.; Xu, X.; Qiao, Z.; Wang, F.; Cai, H.; An, H.; Jia, K.; Liu, Y.; Sun, Z.; Wang, S.; et al. The roles of surrounding 2D/3D landscapes in park cooling effect: Analysis from extreme hot and normal weather perspectives. *Build. Environ.* **2023**, *231*, 107087. [CrossRef]
18. Harbin, L.; Jianguo, W. Use and misuse of landscape indices. *Landsc. Ecol.* **2004**, *19*, 389–399. [CrossRef]
19. Jianguo, W.; Darrel, G.; Alexander, J.; Charles, B.; Redman, L. Quantifying spatiotemporal patterns of urbanization: The case of the two fastest growing metropolitan regions in the United States. *Ecol. Complex.* **2010**, *8*, 1–8. [CrossRef]
20. Tian, Y.; Jim, C.Y.; Tao, Y.; Shi, T. Landscape ecological assessment of green space fragmentation in Hong Kong. *Urban For. Urban Green.* **2011**, *10*, 79–86. [CrossRef]
21. Zhong, Z.H.; Weiqi, Z.H.; Jia, W.; Xiaofang, H.; Yuguo, Q. Sixty-Year Changes in Residential Landscapes in Beijing: A Perspective from Both the Horizontal (2D) and Vertical (3D) Dimensions. *Remote Sens.* **2017**, *9*, 992. [CrossRef]
22. Bin, L.; Baolei, Z.; Le, Y.; Jun, C. Assessing heat risk for residents of complex urban areas from an accessibility-based perspective. *Sustain. Cities Soc.* **2023**, *88*, 104278. [CrossRef]
23. Chen, B.; Xie, M.; Feng, Q.; Li, Z.; Chu, L.; Liu, Q. Heat risk of residents in different types of communities from urban heat-exposed areas. *Sci. Total Env.* **2021**, *768*, 145052. [CrossRef] [PubMed]
24. Wang, X.; Meng, Q.; Zhang, L.; Hu, D. Evaluation of urban green space in terms of thermal environmental benefits using geographical detector analysis. *Int. J. Appl. Earth Obs. Geoinf.* **2021**, *105*, 102610. [CrossRef]
25. Wang, F.; Qin, Z.; Song, C.; Tu, L.; Karnieli, A.; Zhao, S. An Improved Mono-Window Algorithm for Land Surface Temperature Retrieval from Landsat 8 Thermal Infrared Sensor Data. *Remote Sens.* **2015**, *7*, 4268–4289. [CrossRef]
26. Xue, L.; Yuyu, Z.H.; Wenze, Y.; Xuecao, L.; Yong, L.; Debin, L. Spatiotemporal patterns of summer urban heat island in Beijing, China using an improved land surface temperature. *J. Clean. Prod.* **2020**, *257*, 120529. [CrossRef]
27. Bureau, B.S. *Beijing Statistical Yearbook*; China Statistics Press: Beijing, China, 2022.

28. Sun, R.; Chen, L. Effects of green space dynamics on urban heat islands: Mitigation and diversification. *Ecosyst. Serv.* **2017**, *23*, 38–46. [CrossRef]
29. Ke, X.; Men, H.; Zhou, T.; Li, Z.; Zhu, F. Variance of the impact of urban green space on the urban heat island effect among different urban functional zones: A case study in Wuhan. *Urban For. Urban Green.* **2021**, *62*, 127159. [CrossRef]
30. Tu, L.; Qin, Z.; Li, W.; Geng, J.; Yang, L.; Zhao, S.; Zhan, W.; Wang, F. Surface urban heat island effect and its relationship with urban expansion in Nanjing, China. *J. Appl. Remote Sens.* **2016**, *10*, 26037. [CrossRef]
31. Peng, J.; Hu, Y.; Dong, J.; Liu, Q.; Liu, Y. Quantifying spatial morphology and connectivity of urban heat islands in a megacity: A radius approach. *Sci. Total Env.* **2020**, *714*, 136792. [CrossRef]
32. Tran, H.; Uchihama, D.; Ochi, S.; Yasuoka, Y. Assessment with satellite data of the urban heat island effects in Asian mega cities. *Int. J. Appl. Earth Obs. Geoinf.* **2006**, *8*, 34–48. [CrossRef]
33. Soille, P.; Vogt, P. Morphological segmentation of binary patterns. *Pattern Recognit. Lett.* **2009**, *30*, 456–459. [CrossRef]
34. Wei, Q.; Halike, A.; Yao, K.; Chen, L.; Balati, M. Construction and optimization of ecological security pattern in Ebinur Lake Basin based on MSPA-MCR models. *Ecol. Indic.* **2022**, *138*, 108857. [CrossRef]
35. Lian, Z.; Feng, X. Urban Green Space Pattern in Core Cities of the Greater Bay Area Based on Morphological Spatial Pattern Analysis. *Sustainability* **2022**, *14*, 12365. [CrossRef]
36. Chen, A.; Yao, X.A.; Sun, R.; Chen, L. Effect of urban green patterns on surface urban cool islands and its seasonal variations. *Urban For. Urban Green.* **2014**, *13*, 646–654. [CrossRef]
37. Yao, L.; Li, T.; Xu, M.; Xu, Y. How the landscape features of urban green space impact seasonal land surface temperatures at a city-block-scale: An urban heat island study in Beijing, China. *Urban For. Urban Green.* **2020**, *52*, 126704. [CrossRef]
38. Li, X.; Zhou, W.; Ouyang, Z.; Xu, W.; Zheng, H. Spatial pattern of greenspace affects land surface temperature: Evidence from the heavily urbanized Beijing metropolitan area, China. *Landsc. Ecol.* **2012**, *27*, 887–898. [CrossRef]
39. Bao, T.; Li, X.; Zhang, J.; Zhang, Y.; Tian, S. Assessing the Distribution of Urban Green Spaces and its Anisotropic Cooling Distance on Urban Heat Island Pattern in Baotou, China. *ISPRS Int. J. Geo-Inf.* **2016**, *5*, 12. [CrossRef]
40. Yuan, B.; Zhou, L.; Dang, X.; Sun, D.; Hu, F.; Mu, H. Separate and combined effects of 3D building features and urban green space on land surface temperature. *J. Env. Manag.* **2021**, *295*, 113116. [CrossRef]
41. Buyantuyev, A.; Wu, J. Urban heat islands and landscape heterogeneity: Linking spatiotemporal variations in surface temperatures to land-cover and socioeconomic patterns. *Landsc. Ecol.* **2009**, *25*, 17–33. [CrossRef]
42. Kong, F.; Yin, H.; James, P.; Hutyra, L.R.; He, H.S. Effects of spatial pattern of greenspace on urban cooling in a large metropolitan area of eastern China. *Landsc. Urban Plan.* **2014**, *128*, 35–47. [CrossRef]
43. Li, X.; Zhou, W.; Ouyang, Z. Relationship between land surface temperature and spatial pattern of greenspace: What are the effects of spatial resolution? *Landsc. Urban Plan.* **2013**, *114*, 1–8. [CrossRef]
44. Zhou, W.; Huang, G.; Cadenasso, M.L. Does spatial configuration matter? Understanding the effects of land cover pattern on land surface temperature in urban landscapes. *Landsc. Urban Plan.* **2011**, *102*, 54–63. [CrossRef]
45. Aubrecht, C.; Ozceylan, D. Identification of heat risk patterns in the U.S. National Capital Region by integrating heat stress and related vulnerability. *Env. Int.* **2013**, *56*, 65–77. [CrossRef]
46. Musse, M.A.; Barona, D.A.; Santana Rodriguez, L.M. Urban environmental quality assessment using remote sensing and census data. *Int. J. Appl. Earth Obs. Geoinf.* **2018**, *71*, 95–108. [CrossRef]
47. Onishi, A.; Cao, X.; Ito, T.; Shi, F.; Imura, H. Evaluating the potential for urban heat-island mitigation by greening parking lots. *Urban For. Urban Green.* **2010**, *9*, 323–332. [CrossRef]
48. Wang, C.; Wang, Z.-H.; Wang, C.; Myint, S.W. Environmental cooling provided by urban trees under extreme heat and cold waves in U.S. cities. *Remote Sens. Environ.* **2019**, *227*, 28–43. [CrossRef]
49. Li, J.; Song, C.; Cao, L.; Zhu, F.; Meng, X.; Wu, J. Impacts of landscape structure on surface urban heat islands: A case study of Shanghai, China. *Remote Sens. Environ.* **2011**, *115*, 3249–3263. [CrossRef]
50. Yu, Z.; Zhang, J.; Yang, G. How to build a heat network to alleviate surface heat island effect? *Sustain. Cities Soc.* **2021**, *74*, 103135. [CrossRef]